14 Mar 1991, 10:30 am - 12:30 pm

Liquefaction Fragilities for Buried Lifelines

Jose A. Pires
University of California at Irvine, CA

A. H.-S. Ang
University of California at Irvine, CA

I. Katayama
Tokyo Electric Power Services Co. Advanced Engineering Operation Center, Japan

Proceedings: Second International Conference on Recent Advances in Geotechnical Earthquake Engineering and Soil Dynamics, March 11-15, 1991 St. Louis, Missouri, Paper No. 3.64

Liquefaction Fragilities for Buried Lifelines

Jose A. Pires and A. H-S Ang
Department of Civil Engineering University of California at Irvine, Irvine CA

I. Katayama
Tokyo Electric Power Services Co. Advanced Engineering Operation Center Chiyoda-ku, Tokyo, Japan

SYNOPSIS -- For buried structures, such as conduits and underground pipes, liquefaction induced forces will depend on the volume of soil surrounding the structure that will liquefy. Here, a methodology to calculate the probability of the onset of liquefaction at a given depth in a soil deposit is extended to assess the probability that a specified volume of soil will liquefy when liquefaction occurs at a given depth in the deposit. To account for the variability of soil properties with depth, the soil deposit is divided into horizontal layers and the volume of liquefied soil in each layer is calculated as the product of the layer thickness by the lateral extent of liquefaction. Within each layer, the horizontal variability of the soil properties is described by a homogeneous and axisymmetric random field. It is assumed that the ground motions in the horizontal direction are perfectly correlated. The results are presented in terms of the probability of liquefaction spreading over a given area (a circle of radius R) as a function of the intensity of the ground motion.

INTRODUCTION

The first part of the paper describes a methodology to compute the probability of the onset of liquefaction at a given depth in a soil deposit[1]. The probability of liquefaction for the critical depth plotted as a function of the intensity of the ground motions is denoted the liquefaction fragility for the soil deposit. The principal features of the method to compute the probability of the onset of liquefaction in the soil deposit are: (i) the ground motion input is specified at the bottom of the soil deposit; (ii) one-dimensional site amplification analysis is used to account for the effect of local site conditions on the ground accelerations and stresses in the soil deposit and, (iii) makes use of in-situ soil properties and past data on the occurrence or non-occurrence of liquefaction to represent the soil resistance against liquefaction. Additional features of the model are: (i) the ground accelerations are represented by stochastic processes and methods of stochastic structural dynamics are used to compute the statistics of the ground accelerations and shear stresses throughout the deposit; (ii) considers the nonlinear and hysteretic soil behavior and, (iii) includes a transmitting boundary in the one-dimensional lumped-mass model for site amplification studies.

The second part of the paper describes the development of a method to calculate the probability that a specified volume of soil will liquefy when liquefaction occurs at a given depth in the deposit. With the proposed extension, the liquefaction fragility curves will represent the probability of liquefaction over a circle with a specified radius as a function of the intensity of the earthquake ground shaking. Since the adverse consequences of liquefaction for a buried structure (e.g., a conduit) depend on the lateral extent of liquefaction, a realistic definition of liquefaction ought to include this lateral spread.

LIQUEFACTION IN THE LAYER

Ground Response Statistics

The effect of soft soil layers in the severity of shaking in the liquefiable soil layers is evaluated with a one-dimensional ground response analysis which idealizes the site amplification as the result of vertically propagating shear waves. This approach has been shown to offer a reasonably accurate means for estimating site amplification effects for horizontal ground accelerations[2] which are the accelerations of interest in this study. Accordingly, a lumped mass model for the soil deposit (see Fig. 1) is constructed as follows[3]: the soil deposit is divided into a number of elements (layers); the lumped masses, m_i, $i = 1, 2, ..., n+1$, are obtained by lumping one-half the mass of each layer at the layer boundaries and, at the interface between the lowest element and the base only one-half of the mass of the lowest layer is lumped. The motion of the system is described by the total displacements x_i, $i = 1, 2, ..., n+1$, of the layer boundaries. Nonlinear springs with stress-strain properties representing the nonlinear, strain-dependent and hysteretic behavior of the soil connect the massess as shown in Fig. 1. The total shear strain at each layer is defined by $\gamma_i = (x_{i+1} - x_i)/\Delta h_i$.

A number of soil models capable of representing the nonlinear and hysteretic behavior of soils have been proposed [4,5,6]. However, no analytical solutions exists for determining the statistics and probabilities of the soil response to random seismic loadings when the soil behavior is represented by any of the nonlinear-hysteretic soil models mentioned above. A hysteretic model and an analytical solution procedure[7] are proposed here to reproduce the soil hysteresis and also calculate the necessary statistics of the seismic response of horizontally layered soil deposits. The model describes the hysteretic component of the shear stress by a first-order differential equation which allows for a simple linearization of the equations of motion.

The hysteretic component, z, of the shear strain is described by

$$\frac{\partial z}{\partial \gamma} = A - \beta \frac{|\gamma|}{\dot{\gamma}} |z|^{r-1} - \delta |z|^r \qquad (1)$$

where γ is the total shear strain, A, β, δ and r are parameters that describe the shape of the hysteresis loops. The shear stress is given by

$$\tau = \alpha G_m \gamma + (1 - \alpha) G_m z \qquad (2)$$

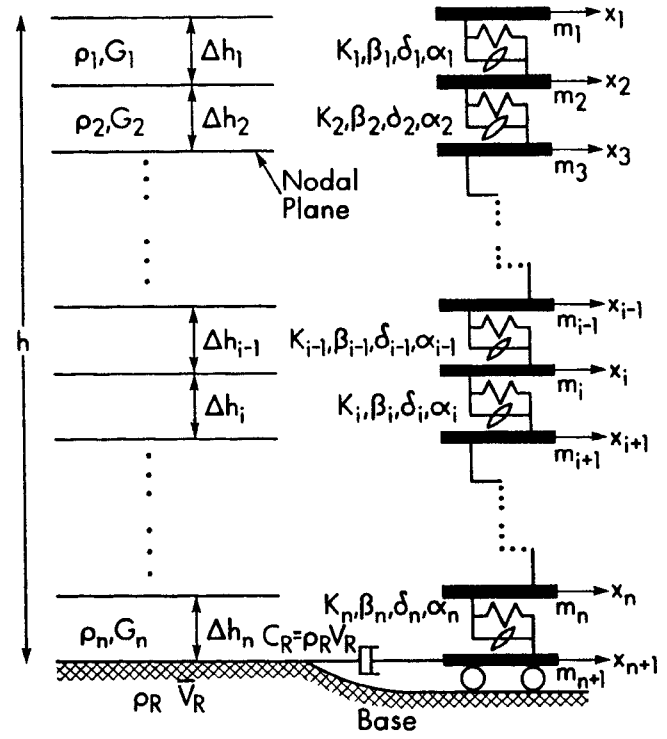

Figure 1 — Lumped Mass Model For Site Amplification Analysis.

where G_m is the (small strains) shear modulus and αG_m is the residual stiffness. The maximum hysteretic shear stress is given by

$$\tau_m = (1-\alpha)G_m[A/(\beta+\delta)]^{1/r} \tag{3}$$

In this study, the following values are used for the parameters of the smooth hysteretic model: $A = 1.0$, $\delta = \beta$, $r = 0.5$ and $\gamma_r = 4.0 \times 10^{-4}$ (where γ_r is a reference strain defined as τ_m/G_m).

Dynamic equilibrium of each lumped-mass requires that, for $i = 1, 2, ..., n$,

$$\begin{aligned} &m_i\ddot{x}_i + (1-\delta_{i1})[\alpha_{i-1}K_{i-1}(x_i - x_{i-1}) + (1-\alpha_{i-1})K_{i-1}(\zeta_i - \zeta_{i-1})] \\ &-[\alpha_i K_i(x_{i+1} - x_i) + (1-\alpha_i)K_i(\zeta_{i+1} - \zeta_i)] = 0 \end{aligned} \tag{4}$$

where $\delta_{i1} = 0$ if $i \neq 1$ and $\delta_{i1} = 1$ if $i = 1$, $K_i = G_{mi}/\Delta h_i$, $i = 1, 2, ..., n$ and $(\zeta_{i+1} - \zeta_i)/\Delta h_i = z_i$ for $i = 1, 2, ..., n$.

For the $n+1$st mass the equation of equilibrium is

$$\begin{aligned} &m_{n+1}\ddot{x}_{n+1} + \alpha_n K_n(x_{n+1} - x_n) + \\ &+(1-\alpha_n)K_n(\zeta_{n+1} - \zeta_n) = \rho_R V_R(2U - \dot{x}_{n+1}) \end{aligned} \tag{5}$$

The term $\rho_R V_R(2U - x_{n+1})$ represents the shear stress that is applied to the bottom of the soil deposit from the underlying stiffer soil or rock base, where ρ_R and V_R are the unit mass and velocity of the shear wave propagation in the underlying base. The term U denotes the input motion in terms of particle velocity from the incident velocity wave[3].

The strong ground motion phase of the earthquake load is represented by a stationary Gaussian random process. In this regard, it can be characterized by a power spectral density function, such as the Clough-Penzien spectrum

$$\begin{aligned} S(\omega) &= S_0 \frac{1 + 4\zeta_B^2(\omega/\omega_B)^2}{[1-(\omega/\omega_B)^2]^2 + 4\zeta_B^2(\omega/\omega_B)^2} \\ &\quad \frac{(\omega/\omega_G)^4}{[1-(\omega/\omega_G)^2]^2 + 4\zeta_G^2(\omega/\omega_G)^2} \end{aligned} \tag{6}$$

To solve for the response statistics the equations of motion are writen as a system of first order differential equations

$$\{\dot{y}\} + [G]\{y\} = \{f\} \tag{7}$$

where the state vector $\{y\}$ contains the relative (between each two consecutive lumped masses) displacements and velocities , plus the hysteretic component of the shear-strain, z_i, for each spring. In addition, the state vector also contains the relative displacements and velocities of the two second-order filters that define the Clough-Penzien power spectrum[8]. The solution for the response requires the determination of the covariance matrix $[S]$, of the response variables satisfying the matrix differential equation

$$[\dot{S}] + [G][S] + [S][G]^T = [B] \tag{8}$$

where $[B]$ is the matrix of the ground motion parameters[7].

Probability of Liquefaction

The resistance of the sand against liquefaction is defined by the number of cycles, $N_\ell(\bar{\tau})$, of constant amplitude shear stress ratio, $\bar{\tau}$, necessary to induce liquefaction; this is known as the "cyclic resistance curve". The shear stress ratio is defined as τ/σ'_{v0}, where τ is the shear stress in the soil and σ'_{v0} is the effective overburden stress. Based on the occurrence of liquefaction during past earthquakes, values of the cyclic shear stress ratio known to have caused liquefaction under a given intensity of shaking have been correlated with a readily available measure of the in-situ condition of the sand, the Standard Penetration Test blowcount normalized to an effective overburden stress of 1.0 ton per sq. ft. and an energy ratio of 60 percent, i.e., $(N_1)_{60} - SPT$[9]. Based on those correlations "cyclic resistance curves" for the sand for various values of the $(N_1)_{60} - SPT$ have been obtained[1]. One such "cyclic resistance curve" is shown in Fig. 2.

Any of the "cyclic resistance curves" can be interpreted by

$$N_\ell(\bar{\tau})[E_c(\bar{\tau})h(\bar{\tau})] = W_u \tag{9}$$

where W_u is an arbitrary constant, $E_c(\bar{\tau})$ is the energy dissipated through hysteresis in one cycle of shear stress amplitude $\bar{\tau}$, and $h(\bar{\tau})$ is a weighing function. The oncept of the number of equivalent uniform loading cycles[9] implies that under N loading cycles with different shear stress, $\bar{\tau}_i$, liquefaction will occur when

$$W = \sum_{i=1}^{N} E_c(\bar{\tau}_i)h(\bar{\tau}_i) \tag{10}$$

reaches W_u. For an earthquake with a given intensity (peak ground acceleration or rms ground acceleration), $A = a$, and a strong motion duration $T_E = t$, liquefaction occurs when

$$Z = W_u - W(a,t) < 0.0 \tag{11}$$

where W_u denotes the hysteretic energy dissipation capacity of the soil layer (liquefaction will be triggered when this energy dissipation capacity is exhausted). The quantity $W(a,t)$ is given by

$$W(a,t) = \int_0^t X(r)\dot{\varepsilon}_T(r)dr \tag{12}$$

where $\dot{\varepsilon_T}(\tau)$ is the rate of hysteretic energy dissipated at time r and $X(r)$ is an equivalent weighing function to include the effect of random stress amplitude[1] which is given by

$$X(r) = [\int_0^{\bar{\tau}_m} h(\bar{\tau}) E_c(\bar{\tau}) f_T(\bar{\tau}, r) d\bar{\tau}] / [\int_0^{\bar{\tau}_m} E_c(\bar{\tau}) f_T(\bar{\tau}, r) d\bar{\tau}] \quad (13)$$

where $\bar{\tau}_m$ is the normalized maximum of the hysteretic component of the shear stress for the sand and $f_T(\bar{\tau}, r)$ is the probability density function of the peaks of $\bar{\tau}$ at time r.

The mean and variance of $W(a,t)$ are obtained from the random vibration analysis, in particular from the mean and variance of the hysteretic energy dissipated[10]. The statistics of W_u are obtained from the uncertainty analysis of the cyclic resistance against liquefaction. On this basis, the "cyclic resistance curves" shown in Fig. 2 are regarded as mean "cyclic resistance curves", and the coefficient of variation of the number of loading cycles that will cause liquefaction at a given stress ratio is independent of the stress ratio and equal to 0.57[1].

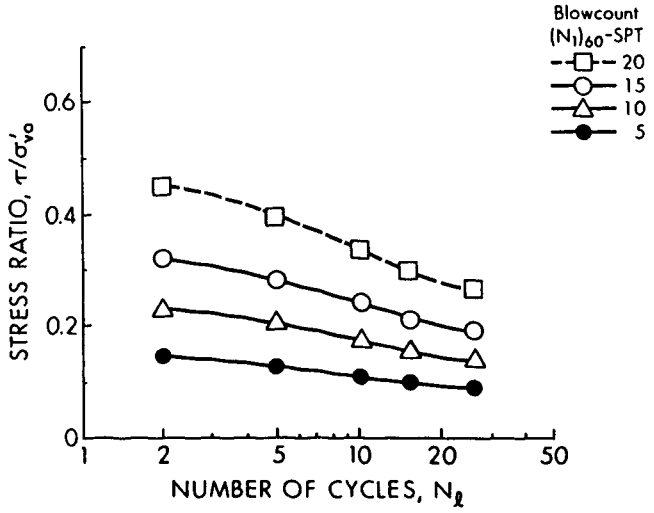

Figure 2 — Cyclic Resistance Curves.

Example Application

Probabilities of the onset of liquefaction under various earthquake load intensities were calculated for the soil deposit shown in Fig. 3. The soil deposit was idealized with the lumped-mass model as indicated in Table 1 below and subjected to the respective levels of earthquake intensities (peak ground accelerations). The parameters of the Clough-Penzien spectrum were chosen to be $\omega_B = 16.9\,rad/sec$, $\zeta_B = 0.94$, $\zeta_G = 0.7$ and $\omega_G = 1.25\,rad/sec$. Figure 4 shows the calculated probabilities of liquefaction as a function of the earthquake intensity and a strong motion duration of 8.0 seconds. It has been previously shown that the probabilities of liquefaction are far less sensitive to the strong motion duration than to the ground motion intensity [1], therefore, the liquefaction fragilities are shown for a given strong motion duration.

To assess the reliability of the method probabilities of liquefaction were computed for some past case histories of occurrence or non-occurrence of liquefaction. The case histories investigated are summarized elsewhere[1]. The results of the investigation are shown in Fig. 5. The line shown in Fig. 5 separates the data for which liquefaction has occurred from those data for which liquefaction has not occurred for 7.5-magnitude earthquakes. The further the data point plots below the line the smaller should be the probability of liquefaction while the further the data point plots above the line the greater should be the probability of liquefaction. The probabilities of the onset of liquefaction computed with the methodology appear to be consistent with the observed data.

Table 1. Lumped-Mass Model for the Soil Deposit Analyzed

Element Number	Element Height (m)	Depth (Midpoint) (m)	σ'_v $(tonf/m^2)$	mass (ton)	Shear Modulus G_m $(tonf/m^2)$
1	1.5	0.75	1.065	2.13	3,710
2	1.5	2.25	3.195	2.13	3,710
3	2.0	4.00	4.680	2.84	3,710
4	2.0	6.00	5.520	2.84	3,710
5	2.5	8.25	6.640	3.90	4,760
6	2.5	10.75	8.040	3.90	4,760
7	2.5	13.25	9.765	4.55	9,210
8	2.5	15.75	11.815	4.55	9,210
9	3.0	18.50	13.680	5.04	11,858
10	3.0	21.50	15.900	5.04	11,858
11	(boundary element with $C_R = 90\,tonf - sec/m$ and a mass of 2.52 ton)				

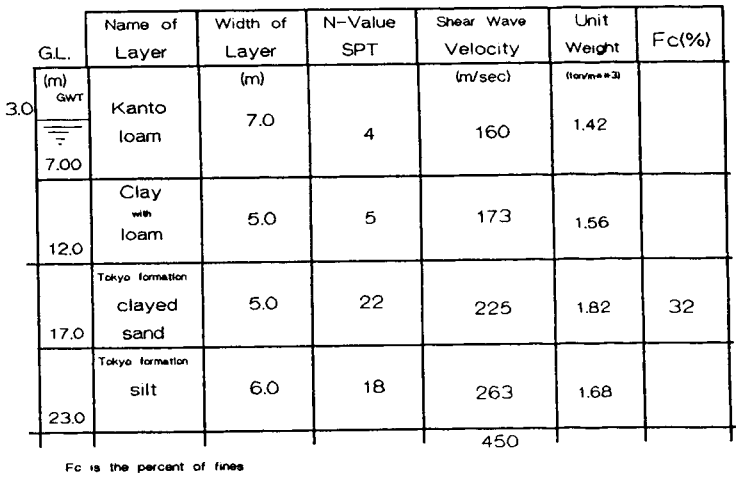

Figure 3 — Soil Deposit Analyzed.

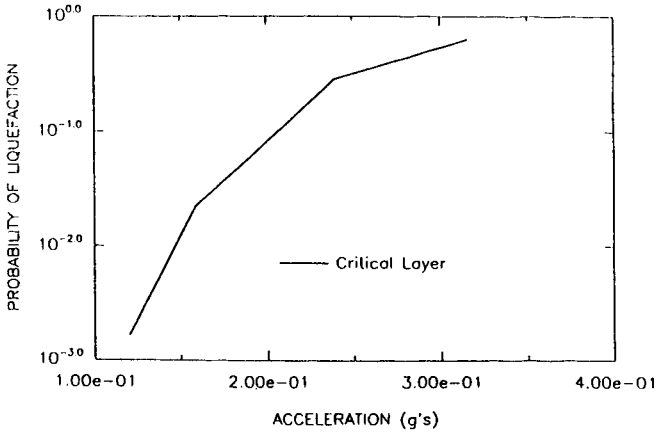

Figure 4 — Liquefaction Fragility (Probability of the Onset of Liquefaction in the Deposit).

DATA CASE	PROBABILITY OF LIQUEFACTION
1	1.000
3	0.954
5	0.460
6	1.000
9_B	0.233
9_T	$2.6\text{x}10^{-5}$
10	0.142
11	$5.8\text{x}10^{-5}$

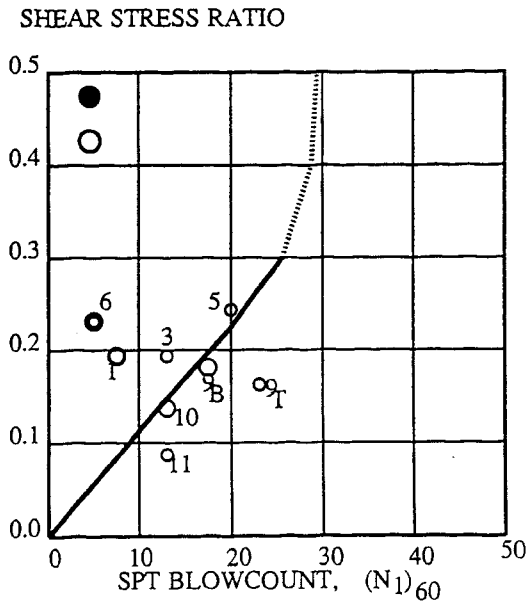

Figure 5 — Probabilities of Liquefaction Computed for Some Data Cases.

LIQUEFACTION SPREAD

Methodology

Consider the soil deposit shown in Fig. 6. The probability that liquefaction will occur at any point in the layer (say point O), independently of what happens anywhere in the layer, is given by

$$P[E_0] = \int_0^\infty F_{W_u}(q) f_{W(a,t)}(q) dq \tag{14}$$

where F_{W_u} denotes is the PDF of W_u and $f_{W(a,t)}$ is the probability density function of $W(a,t)$. To simplify the notation introduce $S = W_u$ and $R = W(a,t)$.

To compute the probability that liquefaction will extend over a circle of radius R (axisymmetric random field), the circle is divided into segments of length D, as shown in Fig. 6 for 5 segments numbered $0, 1, ..., 4$. The soil resistances against liquefaction at the center of each segment are random variables denoted by S_i, $i = 0, 1, ..., 4$. The random variables S_i are identically distributed but are not statistically independent. The correlation coefficients between any pair of random variables S_i, S_j is calculated from the autocorrelation function $R_{SS}(x)$ of the random field $S(x)$ as described below. Suppose that S_i and S_j) are separated by a distance kD where k is a positive integer, then the desired correlation coefficient is

$$\rho_{S,S}(kD) = \frac{R_{S,S}(kD)}{\sigma_{S_i}\sigma_{S_j}} \tag{15}$$

in which $R_{S,S}(x)$ is the autocorrelation function of the random field $S(x)$ and σ_{S_i} is the standard deviation of S_i which is equal to the standard deviation of S_j, σ_{S_j}.

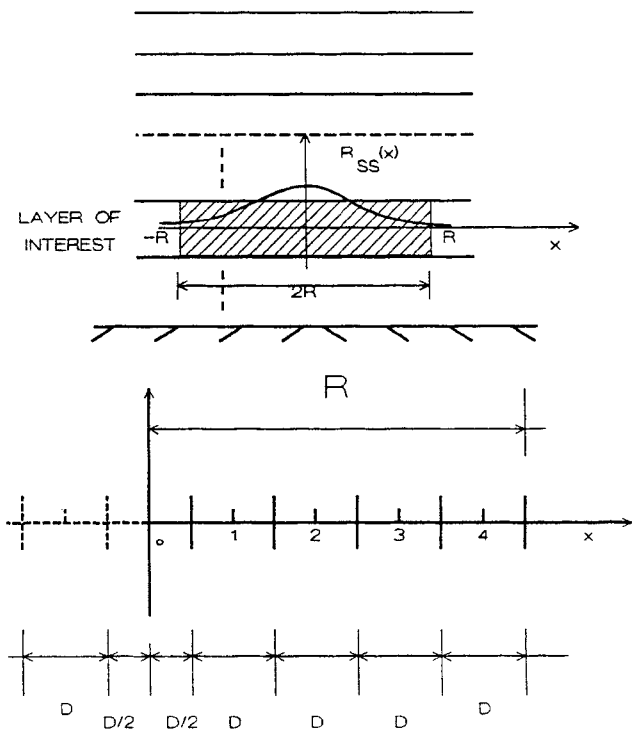

Figure 6 — Idealization of Liquefaction Spread in the Layer.

The probability that liquefaction will extend over the entire circle of radius $R = 4.5D$ is the probability that all segments in the circle will liquefy. Therefore,

$$\begin{aligned} P_L(R = 4.5D) &= Probability[(S_0 < Q) \cap (S_1 < Q) \cap (S_2 < Q) \\ &\quad \cap (S_3 < Q) \cap (S_4 < Q)] \end{aligned} \tag{16}$$

which can be writen as

$$P_L(R = 4.5D) = \int_0^\infty F_{S_0 S_1 S_2 S_3 S_4}(q,q,q,q,q) f_Q(q) dq \tag{17}$$

where

$$\begin{aligned} F_{S_0 S_1 S_2 S_3 S_4}(q,q,q,q,q) &= \int_0^q \cdots \int_0^q f_{S_0 S_1 S_2 S_3 S_4}(s_0, s_1, s_2, s_3, s_4) \\ &\quad dS_0 dS_1 dS_2 dS_3 dS_4 \end{aligned} \tag{18}$$

The random variables S_i may be assumed to follow a lognormal distribution with median S_m and standard deviation σ_{S_i}. The matrix of the correlation coefficients for the random variables S_i is given by

$$[\rho] = \begin{bmatrix} 1.0 & \rho_{SS}(D) & \rho_{SS}(2D) & \rho_{SS}(3D) & \rho_{SS}(4D) \\ & 1.0 & \rho_{SS}(D) & \rho_{SS}(2D) & \rho_{SS}(3D) \\ & & 1.0 & \rho_{SS}(D) & \rho_{SS}(2D) \\ & Symmetric & & 1.0 & \rho_{SS}(D) \\ & & & & 1.0 \end{bmatrix} \tag{19}$$

Evaluation of the multiple integral in Eq. 18 requires numerical integration. All numerical integrations were performed using an adaptive algorithm for numerical integration over an N-dimensional rectangular region[11]. With this algorithm, the numerical integrations can be performed without major difficulties except when the correlation matrix becomes nearly singular.

Example Application

The method described in the previous section is used to compute the newly defined liquefaction fragilities for the soil deposit analyzed. Each liquefaction fragility gives the probability of liquefaction over a circle with a specified radius as a function of the peak ground acceleration.

The correlation function of the soil resistance against liquefaction is assumed to be of the form

$$\rho_{S,S}(x) = exp[-(x/b)^2] \tag{20}$$

where b is a positive parameter. This form of the autocorrelation function has been suggested for some soil properties (e.g., relative density, grain-size distribution and shear strength[12,13]). Other possible forms for the correlation function have also been used [13,14]; e.g.,

$$\rho_{S,S}(x) = exp(-|x|/a) \tag{21}$$

with $a > 0.0$. This second form has the disadvantage that its second derivative at x=0.0 does not exist which implies that the random field representing the soil property is not differentiable. This problem is not present with the form of Eq. 20 which is adopted in this study. Here, b is treated as a parameter and the results are presented as a function of the dimensionless parameter R/b. First, the radius of the circle is fixed ($R = 1.69b$) and the sensitivity of the results to the number of segments in which the circle is subdivided is investigated. Next, the liquefaction fragilities are computed for different radii of the circle. Finally, results showing the probability of liquefaction over a circle with a given radius conditional on the occurrence of liquefaction at the center of the circle are also presented and discussed.

Two, 3, 4 and 5 segments are considered, which correspond to D equal to $1.127b$, $0.676b$, $0.483b$, and $0.376b$, respectively. The computed probabilities of liquefaction are shown in Fig. 7 as a function of the peak ground acceleration. The results shown in Fig. 4 are reproduced in Fig. 7 for reference purposes. The probabilities of liquefaction (over a circle of radius $R = 1.69b$) decrease as the number

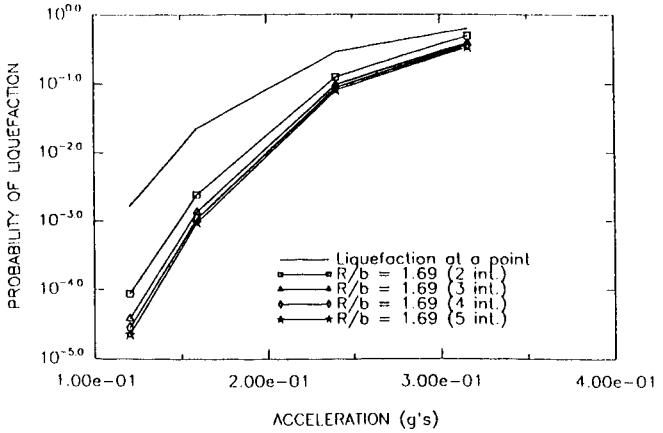

Figure 7 — Probability of Liquefaction Extending Over a Given Area.

of segments increase and appear to converge for $D = 0.376b$. For a smaller D, $D = 0.307b$, the correlation matrix (Eq. 19) becomes almost singular and the integral in Eq. 18 can not be evaluated as accurately as before. Nevertheless, the approximate values were found to be almost identical to those for $D = 0.376b$. As expected, the probability of liquefaction for a circle of radius R is significantly lower than the probability of liquefaction for a single point in the layer.

The probabilities of liquefaction for a peak ground acceleration of 0.24g for three different radii, namely $R = 0.94b$, $R = 1.69b$ and $R = 2.44b$, as given by Eq. 17, are shown in Table 2 in the column labeled Equation 17.

Table 2. Probabilities of Liquefaction for Various Radii

Radius	Equation 17	Approximate Expression
17.8m	0.1583	0.1478
32.0m	0.07868	0.07868
50.3m	0.03867	0.04094

To compute the probability of liquefaction over a circle with radius $R_n = (n + 0.5)D$, where n is a positive integer, an (n+1)-fold integral needs to be evaluated numerically (see Eq. 18). As the radius of the circle increases to $R_{m+n} = (m + n + 0.5)D$, a numerical integration of an (m+n+1)-fold integral is involved. If many different radii need to be considered, the numerical integrations can become very time consuming. Therefore, it is desirable to find a simplified method to compute the probability of liquefaction for a circle of a given radius, say $R_k = (k + 0.5)D$, given that the probability of liquefaction for a circle with radius R_n is known. The following simplified method is proposed:

(i) assume that the probability of liquefaction for a circle with radius $R_n = (n + 0.5)D$ and for a load effect with intensity q can be written as

$$P_L(R_n, q) = F_{S_0}(q)exp[-n\alpha(q)] \tag{22}$$

which can be solved for $\alpha(q)$, obtaining

$$\alpha(q) = \ln[P_L(R_n, q)/F_{S_0}(q)]/(-n) \tag{23}$$

and

(ii) for other radii, $R_k = (k + 0.5)D$, where k is a positive integer, the value of $P_L(R_k, q)$ is

$$P_L(R_k, q) = F_{S_0}(q)exp[-\alpha(q)k] \tag{24}$$

The probabilities of liquefaction over circles with radii, $R = 0.94b$, $R = 1.69b$ and $R = 2.44b$, as computed by Eqs. 22-24, are shown in Table 2 in the column labeled approximate expression. It appears, that for this load intensity, sufficient accuracy is achieved with the approximate procedure.

Figure 8 shows liquefaction fragility curves for cicles with radii, $R = 0.94b$, $R = 2.44b$ (solid lines) computed by Eqs. 22-24 and taking the results for $R = 1.69b$ as the reference values. The same probabilities computed by Eq. 17 are shown in Fig. 8 by dashed lines. It thus appear that the approximate method (Eqs. 22-24) is sufficiently accurate. The results in Fig. 8 also show that the probabilities of liquefaction decrease significantly as the radiius of the circle increases. This last effect seems to be more significant for the lower ground intensities.

Figure 9 shows the conditional probabilities of liquefaction spreading over circles of different radii assuming that liquefaction occurs at the center of the circles. These conditional probabilities of liquefaction are equal to 1.0 at the center of the circle and decrease as the radius of the liquefied zone increases. As the radius increases, the probabilities shown in Fig. 9 decrease more rapidly when the peak ground accelerations are small, i.e., when the probabilities of liquefaction anywhere in the layer are smaller. This implies that the mean size of the liquefied zone will increase if the probability of liquefaction anywhere in the layer also increases.

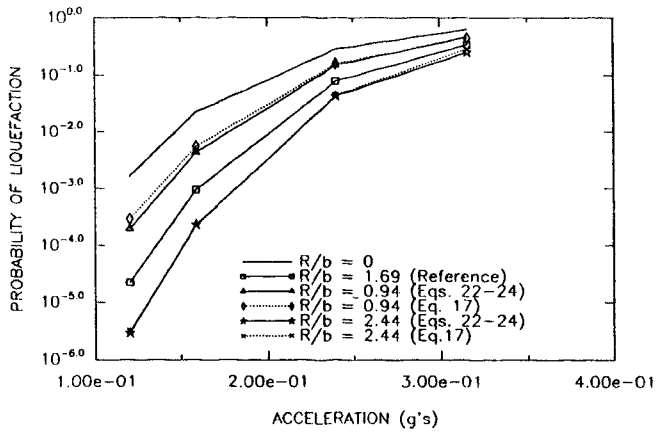

Figure 8 — Probabilities of Liquefaction Spreading Over a Given Area Computed with Eq. 17 and Eqs. 22-24.

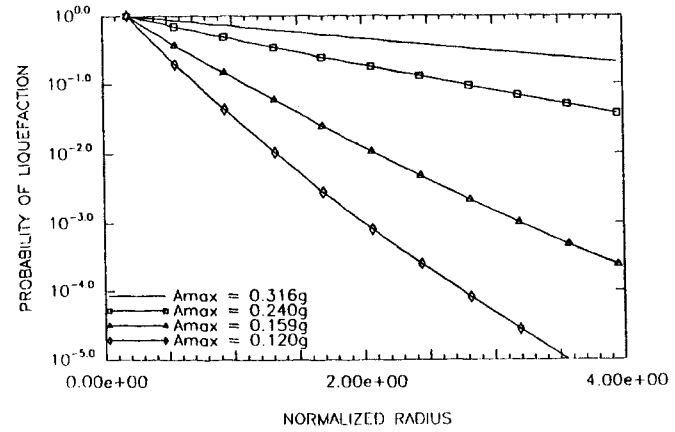

Figure 9 — Probabilities of Liquefaction Spreading Over a Specified Area Conditional on The Occurrence of Liquefaction in its Center.

CONCLUSIONS

A method to calculate the probability of the onset of liquefaction in horizontally layered soil deposits was presented. In general, probabilities of the onset of liquefaction computed with the method are consistent with observed data on occurrence or non-occurrence of liquefaction. The method was extended to compute the probability that liquefaction will spread over a given area. It was observed that the probability that liquefaction will spread over a given area decreases as the contiguous lateral extent of liquefaction increases. Also, the probability that liquefaction will spread over a specified area, on the condition that liquefaction occurs at the center of that area, decreases as the probability of occurrence of liquefaction anywhere in the layer decreases.

References

[1] Pires, J. A., Ang, A. H-S. and Katayama, I., (1989), "Probabilistic Analysis of Liquefaction", in *Structural Dynamics and Soil Structure Interaction*, A.S. Cakmak and I. Herrera, Eds., Computational Mechanics Publications, England.

[2] Idriss, I. M., (1990), "Response of Soft Soils During Earthquakes", presented at the Memorial Symposium to Honor Professor Harry Bolton Seed, Berkeley, CA, May 10-11.

[3] Ishihara, K. and Towhata,I., (1980), "One-Dimensional Soil Response Analysis During Earthquakes Based On Effective Stress Model", Journal of Faculty of Engineering, University of Tokyo, Vol. 35, No. 4.

[4] Finn, W. D. L., Lee, K. and Martin, G., (1977), "An Effective Stress Model for Liquefaction", J. Geotech. Engng., ASCE, 103(6).

[5] Richart, F. E., (1975), "Some Effects of Dynamic Soil Properties on Soil Structure Interaction", J. Geotech. Engng., ASCE, 101(12).

[6] Seed, H. B., Martin, P. P. and Lysmer, J., (1976), "Porewater Pressures During Liquefaction", J. Geotech. Engng., ASCE, 102(4).

[7] Wen, Y. K., (1980), "Equivalent Linearization for Hysteretic Systems Under Random Excitation", J. Appl. Mech., Trans. ASME, 47(1), 150-154.

[8] *Dynamics of Structures*, by Ray W. Clough and Joseph Penzien, McGraw-Hill, New York, 1975.

[9] Seed, H. B. et al, (1984), "The Influence of SPT Procedures in Soil Liquefaction Evaluation", Report No. UCB/EERC-84/15, University of California, Berkeley, California.

[10] Pires, J. A. and Tang, M., (1990), "Statistics of Hysteretic Energy Dissipated Under Random Dynamic Loading", J. Engng. Mech. Div., ASCE, 116(8).

[11] Genz, A. C. and Malik, A. A., "Remarks on algorithm 006: An adaptive algorithm for numerical integration over an N-dimensional rectangular region", Journal of Computational and Applied Mathematics, Vol. 6, No. 4, 1980.

[12] Yamazaki, F. and Shinozuka, M., (1989), "Statistical Preconditioning in Simulation", Proc., ICOSSAR 89, A. H-S. Ang, M. Shinozuka, G. I. Schueller, Eds., ASCE, New York, USA.

[13] Vanmarcke, E., "Reliability of Earth Slopes", Journal of the Geotechnical Engineering division, ASCE, Vol. 103, No. GT11, November, 1977, pp. 1247-1265.

[14] Fardis, M. N. and Veneziano, D., "Estimation of SPT-N and Relative Density", Journal of the Geotechnical Engineering Division, ASCE, Vol. 107, No. GT10, October, 1981, pp. 1345-1359.